Published in final edited form as:
J Neurophysiol. 2007 November ; 98(5): 3023–3033. doi:10.1152/jn.00608.2007.

Nyctalopin Expression in Retinal Bipolar Cells Restores Visual Function in a Mouse Model of Complete X-Linked Congenital Stationary Night Blindness

Ronald G. Gregg[1,2], **Maarten Kamermans**[4], **Jan Klooster**[4], **Peter D. Lukasiewicz**[5], **Neal S. Peachey**[6,7,8], **Kirstan A. Vessey**[2], and **Maureen A. McCall**[2,3]

[1]Department of Biochemistry and Molecular Biology, University of Louisville, Louisville, Kentucky
[2]Department of Ophthalmology and Visual Sciences, University of Louisville, Louisville, Kentucky
[3]Department of Psychological and Brain Sciences, University of Louisville, Louisville, Kentucky
[4]Research Unit Retinal Signal Processing, The Netherlands Institute for Neuroscience, Royal Netherlands Academy of Arts and Sciences, Amsterdam, The Netherlands [5]Department of Ophthalmology and Visual Science, Washington University School of Medicine, St. Louis, Missouri
[6]Research Service, Cleveland Veterans Affairs Medical Center, Cleveland [7]Cole Eye Institute, Cleveland Clinic Foundation, Cleveland [8]Department of Ophthalmology, Cleveland Clinic Lerner College of Medicine of Case Western Reserve University, Cleveland, Ohio

Abstract

Mutations in the *NYX* gene that encodes the protein nyctalopin cause congenital stationary night blindness type 1. In no b-wave (*nob*) mice, a mutation in *Nyx* results in a functional phenotype that includes the absence of the electroretinogram b-wave and abnormal spontaneous and light-evoked activity in retinal ganglion cells (RGCs). In contrast, there is no morphological abnormality in the retina at either the light or electron microscopic levels. These functional deficits suggest that nyctalopin is required for normal synaptic transmission between retinal photoreceptors and depolarizing bipolar cells (DBCs). However, the synaptic etiology and, specifically, the exact location and function of nyctalopin, remain uncertain. We show that *nob* DBCs fail to respond to exogenous application of the photoreceptor neurotransmitter, glutamate, thus demonstrating a postsynaptic deficit in photoreceptor to bipolar cell communication. To determine if postsynaptic expression of nyctalopin is necessary and sufficient to rescue the *nob* phenotype, we constructed transgenic mice that expressed an EYFP-nyctalopin fusion protein on the dendritic tips of the DBCs. Immunohistochemical and ultrastructural studies verified that fusion protein expression was limited to the DBC dendritic tips. Fusion gene expression in *nob* mice restored normal outer and inner visual function as determined by the electroretinogram and RGC spontaneous and evoked responses. Together, our data show that nyctalopin expression on DBC dendrites is required for normal function of the murine retina.

INTRODUCTION

The human retinal disorder, X-linked congenital stationary night blindness type 1 (CSNB1) is caused by mutations in the *NYX* gene, which encodes the protein nyctalopin (Bech-Hansen et al. 2000; Pusch et al. 2000). In addition to a profound loss of rod-mediated visual sensitivity,

Address for reprint requests and other correspondence: R. G. Gregg, Dept. of Biochemistry and Molecular Biology, Center for Genetics and Molecular Medicine, University of Louisville, Delia Baxter Building II, Room 221C, 580 S. Preston St., Louisville, KY 40202 (ron.gregg@louisville.edu).

the CSNB1 phenotype is characterized by the absence of the b-wave component in both the dark and light adapted electroretinogram (ERG), whereas the a-wave is spared (Miyake et al. 1986). The ERG b-wave is generated by the response of depolarizing bipolar cells (DBCs) to a light stimulus (Kofuji et al. 2000; Robson and Frishman 1996), whereas the a-wave reflects the response of photoreceptors (Robson et al. 2003 for review). Therefore the absence of the b-wave in CSNB1 patients indicates a defect in synaptic transmission between photoreceptors and DBCs. A mutant mouse (no b-wave, *nob*) carries a mutation in the murine orthologue of *NYX* (*Nyx*) (Gregg et al. 2003). The *nob* mouse phenotype, which mimics CSNB1 (Pardue et al. 1998) including an absence of the ERG b-wave; a severe loss of rod-mediated visual behavior (Gregg et al. 2003) and an alteration in retinal waves in the immature retina that are critical to development of normal retinal ganglion cell (RGC) function (Demas et al. 2006). These functional abnormalities are not accompanied by morphological changes in the retina, in particular at the synapse between photoreceptors and DBCs (Ball et al. 2003; Pardue et al. 2001).

When the *Grm6* gene, which encodes the expression of the postsynaptic metabotropic glutamate receptor (mGluR6) of DBCs, is inactivated or mutated, mice and patients lack an ERG b-wave (Masu et al. 1995; Pinto et al. 2007; Zeitz et al. 2005b). The similar phenotypes of CSNB1 patients, *nob* mice and GRM6 patients and mice, support the idea that a primary function of nyctalopin involves synaptic transmission between photoreceptors and DBCs. Although patients and mice with mutations in *NYX* and *GRM6* cannot be distinguished using a single flash ERG, it has been shown that patients can be discriminated using a 15-Hz flicker stimulus (Zeitz et al. 2005b). This finding suggests that the two mutations have different downstream consequences on the retinal circuitry and further that mGluR6 and nyctalopin play distinct postsynaptic roles, which could include differential modulation of an unknown nonspecific cation channel on DBCs (Nawy and Jahr 1990).

The role of nyctalopin in synaptic transmission remains unknown. Further, the exact location of nyctalopin expression in the retina has yet to be established although there are reports of its localization to both cellular and synaptic sites (Bahadori et al. 2006; Bech-Hansen et al. 2000; Gregg et al. 2003; Morgans et al. 2006; Pesch et al. 2003). Here we show for the first time in any mouse mutant with a postsynaptic *nob* phenotype that DBCs do not respond to application of exogenous glutamate. Our results show that expression of an EYFP-nyctalopin fusion protein, restricted to *nob* DBCs, rescues both outer and inner visual function. These results indicate that nyctalopin functions postsynaptically at the DBC dendritic tips where it is required for their depolarization via an mGluR6-mediated gating of the nonspecific cation channel in response to a light stimulus.

METHODS

Animals

All experiments were performed using protocols approved by the Animal Care and Use Committee at each institution and the guidelines of the National Institutes of Health and the Society for Neuroscience. The *nob* mutation, originally discovered on the BALBc/ByJ strain (Pardue et al. 1998), has been moved to a C57BL/6J background by more than seven generations of backcrossing. Controls were either littermates or age-matched C57BL/6J mice (The Jackson Laboratory, Bar Harbor, ME). At all institutions, mice were housed in a 12:12 light:dark cycle and were between 6 and 10 wk old at the time of the experiments. For all experimental manipulations, mice were anesthetized with ketamine (80 mg/kg) and xylazine (16 mg/kg) and killed by anesthetic overdose or carbon dioxide exposure.

Transgene construction and generation of transgenic mice

A transgene was constructed using PCR based strategies to attempt to rescue the *nob* phenotype. A promoter fragment, consisting of 8,030 bp of the murine $GABA_C\rho 1$ gene (Gabrr1, Accession No. NM_008075) and ending at position 98 was used to drive expression of the fusion gene in BCs. The fusion gene also contained a Kozak sequence (Kozak 1991) fused to the open reading frame of a cDNA representing the murine *Nyx* gene (Accession No. NM_173415). The open reading frame of EYFP was inserted in-frame after the codon for amino acid 19 of the nyctalopin protein (Gregg et al. 2003). To improve expression, a rabbit β-globin fragment containing the 3′ 19 bp of exon 2, intron 2, and exon 3 and a polyadenylation signal (Brinster et al. 1985) were placed downstream of the EYFP-Nyx fusion construct. The final construct was verified by sequencing. Transgenic mice were generated by standard pronuclear injection procedures and founders identified by PCR of DNA isolated from tail snips. Twelve founder lines were generated and one, designated as *Tg(Gabrr1:EYFP-Nyx)*^{Rgg1}, was used in the studies described here. *Tg(Gabrr1:EYFP-Nyx)*^{Rgg1} males were crossed to *Nyx*$^{nob/nob}$ females to obtain *Nyxn*$^{ob/Y}$ and *Nyxn*$^{ob/Y}$*;Tg(Gabrr1:EYFP-Nyx)*^{Rgg1} animals. For brevity and clarity *Nyx*$^{nob/nob}$ females and *Nyxn*$^{ob/Y}$ males, will be referred to as *nob* mice and *Tg(Gabrr1:EYFP-Nyx)*^{Rgg1}; Nyxn$^{ob/Y}$ males will be referred to as *nob* rescue mice.

Whole cell patch-clamp recordings

Details of the whole cell patch-clamp recording protocols from mouse retinal bipolar cells have been published (Lukasiewicz and Roeder 1995; McCall et al. 2002). Mice were killed by exposure to CO_2, and their eyes were enucleated. The cornea, lens, and vitreous were removed, the retina was dissected, and slices were made under normal room light. Slices were maintained in cold, oxygenated normal mouse Ringer solution, which contained (in mM) 137 NaCl, 2 KCl, 1 $MgCl_2$, 2.5 $CaCl_2$, 28 glucose, and 10 HEPES, until used. Whole cell patch recordings were obtained from BCs in light-adapted retinal slices, using electrodes filled with Lucifer yellow dissolved in the internal solution (see following text) to permit imaging and classification of each BC based on its morphology as well as the locations of its cell body, and axonal and dendritic arbors (Ghosh et al. 2004). After break-in, BCs were voltage-clamped at a holding potential of −60 mV. Electrodes were pulled from borosilicate glass (1B150F-4; World Precision Instruments, Sarasota, FL) on a P97 Flaming/Brown puller (Sutter Instruments, Novato, CA) and had measured resistances of <2–3 MΩ. The internal electrode solution contained (in mM) 127 potassium gluconate, 10 sodium HEPES, 10 BAPTA, 4 Mg-ATP, and 1 Li-GTP. Glutamate (1–5 mM) was puffed (100-ms duration) onto the labeled dendritic terminals of BCs with a Picospritzer at 45- or 60-s intervals. Patchit software (White Perch Software, Somerville, MA) was used to generate voltage command outputs, acquire data, and trigger the Picospritzer (General Valve, Fairfield, NH). The data were digitized and stored using a Labmaster DMA data acquisition board (Scientific Solutions, Solon, OH). Responses were filtered at 1 kHz with the four-pole Bessel low-pass filter on the Axopatch 200B (Axon Instruments, Foster City, CA) and sampled at 1–2 kHz. Mean current amplitude and current variance were measured in the absence or presence of glutamate with Tack analysis software (White Perch Software, Somerville, MA) over 500-ms intervals. Paired Student's *t*-tests were used to compare control and glutamate responses in the same DBC. Unpaired Student's *t*-tests, assuming unequal variance, were used to compare responses across different populations of DBCs. Data for rod and cone DBCs were combined for comparisons because no differences in responses between these groups were observed. Differences were considered significant when $P < 0.05$.

Confocal and electron microscopy—immunohistochemistry

For confocal microscopy, freshly dissected retinas were immersion fixed for 15–20 min in 4% (wt/vol) paraformaldehyde in 0.1 M phosphate buffer (PB), pH 7.4. They were then washed

in PB, cryoprotected through a graded sucrose series, and frozen in OCT (Sakura Finetek, Torrence, CA):20% sucrose (2:1) (Barthel and Raymond 1990). Twelve-micrometer sections were cut on a cryostat, mounted onto Super-Frost glass slides, air-dried and stored at −80°C. Sections were brought to room temperature (RT) and incubated in blocking solution containing: 5% (vol/vol) normal horse serum, 0.5% (vol/vol) Triton X-100 in PB for 30 min. Primary antibodies were diluted in blocking solution and incubated with the section on slides at RT overnight. Antibodies and their dilutions are as follows: anti-ctbp2/ribeye (BD Biosciences Pharmingen, San Diego, CA, at 1:1,000); rhodamine-labeled peanut agglutinin (PNA, Vector Labs, Burlingame, CA, at 1 μg/ml); anti-mGluR6 (Neuromics, Edina, MN, at 1:1,000), EYFP-nyctalopin was detected with either rabbit anti-GFP antibodies conjugated to Alexa 488 or mouse anti-GFP antibodies (Invitrogen, Carlsbad, CA, both at 1:1,000). After incubation with the primary antibody, sections were washed in PB three times for 20 min, sections were incubated in fluorescent secondary antibodies (1:1,000) at RT for 1 h. Secondary antibodies (Invitrogen, Carlsbad, CA) were Alexa 488 goat anti-mouse and Alexa 488 and 568 goat anti-rabbit. Slides were then washed three times in PB and cover-slipped with Immunomount (ThermoShandon, Pittsburgh, PA). Immunostained sections were imaged on an Olympus FV300 confocal microscope, using a 60× oil objective (1.42 NA). Images shown are maximum projections of confocal stacks, adjusted for contrast and brightness with Adobe Photoshop v9.0.1.

For electron microscopy (EM), anesthetized mice were perfused transcardially with heparinized PBS (1 U/ml), followed by 4% paraformaldehyde in PB. The eyes were removed and postfixed for 45 min in 4% paraformaldehyde in PB. After rinsing in PB, the eyes were cryoprotected at RT in 12.5% sucrose in PB for 30 min, then 25% sucrose in PB for 1 h, and afterward frozen in OCT. Frozen sections of 30–40 μm were cut on a freezing microtome and collected in PB. The sections were incubated for 96 h with diluted antisera against GFP (1:500) or mGluR6 (1:1,500, Neuromics, Edina, MN). After rinsing, sections were incubated in a PowerVisionPoly-HRP-Goat anti mouse IgG or a PowerVisionPoly-HRP-Goat anti rabbit IgG (Immunovision Technologies, Dale City, CA). To visualize the peroxidase, sections were incubated in a Tris-HCl diaminobenzidine (DAB) solution containing 0.03% H_2O_2. Subsequently, the DAB reaction product was intensified by the gold substituted silver peroxidase method (van den Pol and Gorcs 1986). Sections were rinsed in 0.1 M sodium cacodylate buffer (pH 7.4) and postfixed for 20 min in 1% OsO_4 supplemented with 1% potassium ferricyanide in sodium cacodylate buffer 0.1 M (pH 7.4) The material was dehydrated and embedded in epoxy resin. Ultrathin sections were observed in a Technai G2 electron microscope (FEI). Photographs were obtained in TIFF format with a MEGAVIEW III camera and were optimized for brightness and contrast in Adobe Photoshop 9.0.1.

Electroretinography

Details of the ERG procedures have been published elsewhere (Chang et al. 2006). After overnight dark adaptation, mice were anesthetized, their corneas were topically anesthetized (1% proparacaine HCl), and their pupils were dilated (1% mydriacyl, 2.5% phenylephrine HCl, 1% cyclopentolate HCl), and body temperature was maintained at 37°C. ERGs were recorded using a stainless steel electrode that contacted the corneal surface through a layer of 0.7% methylcellulose. Responses were differentially amplified, band-pass filtered (0.05–1,500 Hz), averaged and stored using a UTAS E-3000 signal averaging system (LKC Technologies, Gaithersburg, MD). Stimulus flashes (−3.6-2.1 log cd s/m^2) were first presented to the dark-adapted eye in order of increasing intensity, and at least two successive responses were averaged for each flash intensity with interstimulus intervals (ISIs) appropriate to maintain a stable response. For photopic responses, an adapting field consisting of a steady rod-desensitizing background (1.48 log cd/m^2) was presented for 7 min prior to collecting light-adapted ERG data. Flashes (−0.8–1.9 log cd s/m^2) were superimposed on the adapting field

and responses to 100 flashes presented at 2.1 Hz were averaged at each intensity level. The amplitude of the a-wave was measured from the prestimulus baseline to the a-wave trough. The amplitude of the b-wave was measured from the a-wave trough to the peak of the b-wave or, if no a-wave was present, from the prestimulus baseline.

In vivo extracellular recordings

All procedures have been described elsewhere (Chang et al. 2006; Sagdullaev and McCall 2005; Sagdullaev et al. 2006). Anesthetized mice were mounted in a sterotaxic frame, and their body temperature is maintained at 37°C with a thermistor-controlled heating pad. Topical Mydfrin and Mydriacyl (phenylephrine hydrochloride ophthalmic solution, 2.5%, and tropicamide ophthalmic solution, 1%, respectively; Alcon Labs, Fort Worth, TX) were applied to dilate the pupils and paralyze accommodation. A drop of 2.5% hydroxypropyl methylcellulose solution (Goniosol, CIBAVision Ophthalmics) in artificial tears; Teargen, Goldline) was used in conjunction with clear zero-power contact lenses to protect the corneas from drying and to deter cataract formation. The clarity of the optics was checked periodically, and as published previously, we also observed that corrective lenses did not alter RF center diameters (Artal et al. 1998; Balkema and Pinto 1982; Sagdullaev and McCall 2005). Action potentials were recorded extracellularly from single optic nerve axons, using tungsten microelectrodes coated with varnish (impedance: 30–90 MΩ approximately at 12 Hz). Action potentials were isolated, amplified (X3-Cell, slope/height window discriminator/amplifier, FHC, Bowdoinham, ME), digitized at 15 kHz (Power1401, CED), and stored for off-line analyses. Isolated spike trains were both displayed on a computer monitor (Spike2, CED) and played over an audio-monitor (AM7, Grass Instruments, Quincy, MA) so that direct feedback of the cell's response to each visual stimulus was obtained.

After each RGC was isolated, its receptive field (RF) and center sign were determined. Spontaneous responses were recorded either in complete darkness or with a CRT display monitor (Eizo E120 Flex-Scan FXC7) set to different adaptation levels. Evoked responses were elicited using visual stimuli (VisionWorks; Vision Research Graphics, Durham, NH) presented on the monitor the distance of which was 25 cm from the anterior nodal point of the eye. Spontaneous and evoked responses to full-field stimuli were characterized initially under light adapted conditions and then recharacterized after a period of dark adaptation. Specifically, spontaneous activity was recorded for 5 min at an adaptation level of 75 cd/m^2. Evoked responses were then recorded to a full-field stimulus the luminance of which was continuously square-wave modulated between 0 and 150 cd/m^2, for 30 presentations. The room was then completely darkened and the retina allowed to dark adapt for 20 min, which we have empirically determined sufficient to drive responses via the rod pathway (G. L. Yarbrough and M. A. McCall, unpublished observations). Spontaneous activity was then measured for 5 min, in the absence of any light. Evoked responses were then recorded to a full-field stimulus whose luminance was continuously square-wave modulated between 0 and 3 cd/m^2.

The RF extent and organization of each RGC was assessed using two quantitative methods: an area response function (ARF) and a matrix response function (MRF). These experiments were performed only at light-adapted levels, where the independent function of the ON and OFF pathways can be compared. Generation and analyses of the ARF has been described previously (Sagdullaev and McCall 2005). Briefly, RGC responses were recorded to a series of computer generated spot stimuli centered on the cell's RF center and square-wave modulated to either 0 cd/m^2 (for OFF-center RGCs) or 50 cd/m^2 (for ON-center RGCs) around a mean background of 25 cd/m^2. Spots of varying diameter (4.4–52°) were presented in random order for eight trials for a duration of 2 s followed by a 5 s ISI. MRFs were generated to produce three-dimensional (3D) RF maps with response amplitude plotted on the *z* axis as a function of the position of the spot on the display monitor. Spots (diameter = 9°) were generated and systematically

appeared at consecutive overlapping positions across the display monitor in 6 × 8 grid (48 sites). Spot luminance was square-wave modulated around a mean background (20 cd/m^2) to either 3 cd/m^2 (OFF-center RGCs) or 100 cd/m^2 (ON-center RGCs) and its duration, again, was 2 s with a 5 s ISI. Responses to five presentations of each stimulus were averaged, and the mean of the response over the first 400 ms after stimulus onset plotted against spot location. The 3D matrix was smoothed to create a color-coded surface map of the cell's RF using custom built software in Matlab (version 6.5, MathWorks, Natwick, MA).

Light-adapted intensity response functions (IRFs), as previously described (Chang et al. 2006; Sagdullaev et al. 2006), also were used to examine response gain. Responses were recorded to an optimally sized spot whose luminance varied from 30 to 1680 cd/m^2 for ON-center RGCs and from 30 to 0 cd/m^2 for OFF-center RGCs in 0.25–0.5 log intensity steps. Between steps the screen luminance returned to background (30 cd/m^2). ISIs were varied to maintain response consistency at each intensity step from 10 s for the low-intensity changes to ≤60 s for the highest-intensity changes.

For quantitative characterizations, RGC responses were accumulated with a 1-ms bin width. Individual responses were displayed as raster plots and average responses as peristimulus time histograms (PSTHs; 50-ms bin width), which were smoothed (100-ms bin width) to permit measurement of various response parameters (e.g., time to peak, peak response, etc). From the spontaneous activity, the mean spike rate was estimated and a fast Fourier transform (FFT) performed to extract the power spectra.

RGC responses were collected from five to seven mice of each genotype, and cells were grouped according to either their full-field (ON, OFF, or ON-OFF) or RF center (ON- or OFF-center) responses. Unpaired Student's *t*-tests were used to compare groups of RGCs from different genotypes, and paired *t*-tests were used to compare responses from the same RGC under different stimulation conditions (e.g., light- vs. dark-adapted). Differences were considered significant when $P < 0.05$.

RESULTS

Glutamate evokes responses from hyperpolarizing but not depolarizing BCs in nob retina

In *nob* mice, the presence of an ERG a-wave with normal leading edge kinetics indicates that photoreceptor transduction is unaffected. In contrast, the absence of a b-wave in these mice indicates that synaptic transmission is abnormal. This could be due to altered release of the photoreceptor neurotransmitter, glutamate and/or the lack of a DBC response due to the absence of a critical component of their mGluR6 receptor-mediated signal transduction. To address whether pre- or postsynaptic function is defective in *nob* mice, we voltage clamped the bipolar cells to −60 mV and characterized the responses of control and *nob* BCs to exogenous glutamate puffs applied to their dendrites. Lucifer-yellow-filled BCs were classified as rod or cone DBCs and cone hyperpolarizing bipolar cells (HBCs) (Ghosh et al. 2004). Consistent with previous reports (Nawy and Jahr 1990; Shiells and Falk 1990) all control DBCs (rod, $n = 6$; cone, $n = 4$) exhibited a robust outward current in response to a glutamate puff. This is consistent with earlier reports (Nawy and Jahr 1990; Wilson et al. 1987) (Fig. 1*B*) and reflects closure of the nonspecific cation channel. Control HBCs ($n = 2$) exhibited a robust but transient inward current (Fig. 1), reflecting the opening of AMPA/kainate type ionotropic receptors. Similarly, every *nob* HBC ($n = 5$) also showed a transient inward current whose response kinetics were similar to controls. In contrast, *nob* DBCs (rod, $n = 10$; cone, $n = 9$) failed to respond to glutamate puffs, e.g., no current was evoked, even when responses could be elicited from HBCs in the same retina.

The absence of glutamate induced currents in *nob* DBCs could occur if the cation channel was closed or was absent. To examine these possibilities, we determined the amplitude of inward holding currents in *nob* DBCs in the absence and presence of glutamate and determined the open probability of the cation channel using noise analyses. The holding currents in control DBCs were inward, whereas the currents in *nob* DBCs were very small and outward (Fig. 1*B*). These findings suggested that the mGluR6-gated cation channels were mostly closed in *nob* DBCs and open in control DBCs.

To assess the probability of channel opening, we measured and compared the current variance in control and *nob* DBCs. As a rule, current variance is high when the probability of channel opening is 0.5 and is low when channels are either all open or all closed. In control DBCs, glutamate reduced the current variance (Fig. 1*C*), reflecting channel closure; this is consistent with earlier studies (Wilson et al. 1987). The current variance of *nob* DBCs was always lower than in control DBCs, both in the absence or presence of glutamate (Fig. 1*C*), indicating either a low or very high channel open probability. Combining the observations that the cation channel mediated currents in the *nob* DBCs is very low and the variance data that the open probability is also low, suggest the channel is either mostly closed or absent. These data demonstrate a clear postsynaptic defect in *nob* DBCs that results in an inability of the cell to respond to neurotransmitter. However, they do not preclude an additional presynaptic abnormality.

Expression of a nyctalopin fusion protein is restricted to the dendritic terminals of BCs

Our previous ERG characterizations and our current patch-clamp results are consistent with the hypothesis that nyctalopin expression is required for mGluR6-mediated gating of the cation channel in DBCs but is not needed for AMPA/kainate-mediated responses in HBCs. Our previous observations in *nob* mice also have shown significant retinal defects downstream of DBC malfunction. Specifically, in vitro multielectrode array recordings from *nob* RGCs, after eye opening, show abnormal rhythmic spontaneous bursting, as well as abnormal visually evoked responses to full-field stimulation (Demas et al. 2006). Conflicting reports regarding the location of nyctalopin expression (Bahadori et al. 2006; Bech-Hansen et al. 2000; Gregg et al. 2003; Morgans et al. 2006; Pesch et al. 2003) suggest that nyctalopin also could function downstream of the DBC response in the retina. To differentiate between these possible effects, we generated a transgenic mouse line that expressed an EYFP-nyctalopin fusion protein under the control of the murine GABAcρ1 promoter, which we have used previously to express GFP throughout the entire BC and in all BC classes (rod and cone DBCs and cone HBCs) (M. A. McCall, unpublished observations). This promoter was chosen over others like mGluR6 or GαO, which might yield higher expression levels restricted to DBCs because we wanted to limit overexpression of EYFP-nyctalopin, which could interfere with normal localization of the protein and/or cause unexpected secondary defects.

The retinal distribution of the EYFP-nyctalopin fusion protein was examined using immunohistochemistry. When retinal sections of control and *nob* rescue mice were incubated with an anti-GFP antibody, which also recognizes EYFP, we found robust EYFP-nyctalopin expression limited to the outer plexiform layer (OPL) in all transgenic animals (Fig. 2*C*). Even at high magnification, the staining of EYFP-nyctalopin is restricted to puncta consistent with their location on DBC dendrites (Fig. 3*A*). No expression was ever seen in nontransgenic *nob* control retinas (Fig. 2*B*). Because rod DBCs outnumber cone DBCs in the mouse retina, much of this EYFP expression must be localized at the rod to rod DBC synapse. However, both rod and cone DBC function is abnormal in *nob* mice (Fig. 1; ERG) (Krishna et al. 2002;Pardue et al. 1998). To evaluate whether the fusion protein also was expressed at the cone to cone BC synapse, we reacted retinal sections with antibodies to both GFP (for the transgene) and peanut agglutinin (PNA), a lectin expressed on cone pedicles. Figure 2, *D–F*, shows representative expression patterns of these two markers and their co-localization in sections

from *nob* rescue mice. In the merged image (Fig. 2*F*), co-localization of EYFP-nyctalopin and PNA is evident, and the pattern is consistent with alignment of the cone terminal with invaginating BC dendrites within the synaptic space. These data also are consistent with the predicted extracellular location of nyctalopin and the membrane associated and extracellular location of the lectin stained by PNA (Blanks et al. 1993;Johnson et al. 1986). The remaining EYFP-nyctalopin-positive puncta (green) in the merged image represent expression at the smaller rod to rod DBC synapse. Given the selective nature of $GABA_C\rho 1$ expression to retinal BCs (Enz et al. 1996; McCall, unpublished observations), and our co-localization results, it is most likely that the EYFP-nyctalopin fusion gene expression is postsynaptic to the photoreceptor terminals and, in particular, to the BC dendritic tips where they synapse with rod and cone photoreceptors.

To more accurately determine the location of the EYFP-nyctalopin fusion protein, we examined retinal sections for co-expression of the fusion protein with several other well-characterized markers located on the pre- and postsynaptic membrane at this synapse. Figure 3, *A–C*, illustrates the expression pattern of EYFP-nyctalopin (green) and ribeye (red), a protein that is an integral part of the presynaptic ribbon located in the photoreceptor terminals. In the merged images (Fig. 3*C*), it is obvious that ribeye and EYFP-nyctalopin do not co-localize but that they are closely associated. Figure 3, *D–F*, shows the expression pattern of EYFP-nyctalopin (green) and calbindin (red), a protein expressed on invaginating horizontal cell processes. In the merged images (*F*), the horizontal cell dendrites almost completely surround EYFP-nyctalopin-positive puncta but, again, do not co-localize. It should be noted that background staining in Fig. 3, *D* and *G* (asterisks), results from the use of a mouse anti-GFP antibody and an anti-mouse IgG secondary antibody. Figure 3, *G–I*, illustrates the expression patterns of EYFP-nyctalopin (green) and mGluR6 (red), the glutamate receptor expressed on DBC dendrites postsynaptic to the ribbon synapse (Vardi et al. 2000). The staining patterns of both proteins are limited to the OPL and appear as puncta (Fig. 3, *G* and *H*, respectively), and their merged images show nearly complete co-localization (Fig. 3*I*). These data also are consistent with EYFP-nyctalopin localization on the dendrites of DBCs in close association with mGluR6.

To further refine the postsynaptic location of EYFP-nyctalopin, we used preembedding immuno-EM and compared its expression pattern with mGluR6 in *nob* rescue mice. Consistent with our confocal results and those of Vardi et al. (2000), mGluR6 immunoreactivity is concentrated in the invaginating DBC dendrites postsynaptic to ribbon synapses in cone (Fig. 4*A*) and rod (Fig. 4*B*) photoreceptors, although some staining is present throughout the proximal dendrites of the DBCs. Expression of EYFP-nyctalopin in rod spherules is found exclusively on postsynaptic BC dendrites (Fig. 4, *D* and *E*), but its pattern differs from mGluR6 in two ways. First, EYFP-nyctalopin expression is restricted to the region of the BC membrane and, in many cases appears to be extracellular, consistent with our in silico predicted location of the amino terminal end of nyctalopin and, therefore, EYFP (Gregg et al. 2003). Second, although EYFP-nyctalopin expression is seen within the invaginating synapse, in many cases, its expression also can be found distal to the site of contact with the synaptic ribbon (see Fig. *4E*), unlike mGluR6, which is always located proximal to the ribbon. Data from cone terminals indicate EYFP-nyctalopin is frequently at the base of the terminal (Fig. 4*C*). This is slightly more distal to the invaginating synapse than the staining for mGluR6, which fills the terminal of the DBC (Fig. 4*A*). Although these two markers do not appear to overlap at the base of the cones in the EM images, the distance between the two is <200 nm. This is beyond the resolution of the confocal microscope hence mGluR6 and EYFP-nyctalopin co-localize in the merged confocal images (Fig. 3*I*). This location also places EYFP-nyctalopin close to the location stained by PNA. We believe the staining at the base of the cone terminals is in cone DBCs because the light-adapted ERG is restored in the *nob* rescue mice. Further, if HBCs also

expressed EYFP-nyctalopin, we would expect all the processes at the base of cone terminals to be stained, and this is clearly not the case (Fig. 4*C*).

Taken together, our confocal and EM results place expression of the EYFP-nyctalopin fusion protein postsynaptically on the dendrites of DBCs. Further, EYFP-nyctalopin protein expression is most likely closely associated with mGluR6 but possibly within the extracellular space, an assertion that requires further experiments.

Expression of nyctalopin fusion protein on DBC dendrites restores visual function in the outer and inner retina

Although our results indicate postsynaptic expression of nyctalopin, as well as, a postsynaptic defect in DBC function in *nob* mice, our data do not eliminate an additional presynaptic effect. Further, our observations that spontaneous activity and visually-evoked responses to full field flashes are abnormal in *nob* RGCs (Demas et al. 2006), could result from an absence of nyctalopin expression in the inner retina, downstream from the DBC defect. Because our immunohistochemical results show that EYFP-nyctalopin protein expression is limited to the DBC dendritic tips, we used *nob* rescue mice to answer two questions: is postsynaptic expression of nyctalopin (in the form of the fusion protein) sufficient to restore the ERG b-wave and is postsynaptic expression of nyctalopin sufficient to restore downstream visual function?

Using the ERG, we examined responses of control and *nob* rescue mice under dark-adapted conditions. In control mice (Fig. 5, *A* and *B*), the ERG evoked by low-intensity flashes consists of a b-wave on which are superimposed oscillatory potentials (OPs) that reflect inner retinal activity (Ogden 1973; Wachtmeister and Dowling 1978). At higher flash intensities, a negative polarity a-wave precedes the b-wave. In *nob* mice regardless of flash intensity, the dark-adapted ERG has neither a b-wave nor OPs (Pardue et al. 1998). In contrast, in *nob* rescue mice both the b-wave and OPs are fully restored (Fig. 5*A*), and averaged a- and b-wave intensity-response functions (Fig. 5*B*) demonstrate that each component is comparable to controls. Light-adapted ERGs, reflecting the activation of DBCs through the cone pathway, also are abnormal in *nob* mice but, similar to dark-adapted results, *nob* rescue ERGs are again comparable to controls (Fig. 5, *C* and *D*). These data show that expression of EYFP-nyctalopin on the dendritic tips of DBCs fully restores the outer retina defects in *nob* mice that are assessed by the ERG. These data support our assertion that only postsynaptic expression of nyctalopin is required for DBC function.

We recorded the spontaneous and visually evoked responses of *nob* rescue RGCs and compared them to controls recorded under the same conditions. The abnormalities in both spontaneous and evoked responses of RGCs in *nob* mice that we reported previously, rhythmic spontaneous bursting and decreased sensitivity (Demas et al. 2006), were completely resolved by the expression of the EYFP-nyctalopin fusion protein.

Qualitatively, none of the *nob* rescue RGCs exhibited rhythmic spontaneous bursting. Figure 6 compares the spontaneous activity of *nob*, control, and *nob* rescue RGCs. The rhythmic bursting of the majority of *nob* RGCs is evident in five of the six cells shown in Fig. 6*A*. In contrast, the spontaneous activity in control and *nob* rescue RGCs appears random (Fig. 6, *B* and *C*). Quantitatively, fast Fourier transform (FFT) can be used to determine the burst frequency underlying the activity and in the majority of *nob* RGCs this is ~4.5 Hz. FFT analyses of the spontaneous activity of control and *nob* rescue RGCs only reveals a peak at 0 Hz, indicating the absence of rhythmic activity (data not shown).

In the *nob* retina, a large proportion of RGCs are unresponsive to light stimulation (Fig. 6*D*) (Demas et al. 2006), and those with visually evoked responses exhibit bursting superimposed

on their evoked response to a full-field stimulus (Fig. 6*D*). RGCs in *nob* rescue retina were all visually responsive and full-field stimulation yielded robust, short-latency responses identical to controls (Fig. 6, *E* and *F*). The responses of *nob* rescue RGCs to full-field stimulation could be divided into three classes: response at light onset only (ON; $n = 22$ control; $n = 21$ *nob* rescue), response at light offset only (OFF; $n = 6$ control; $n = 5$ *nob* rescue) and response at both light onset and offset (ON-OFF; $n = 8$ control; $n = 5$ *nob* rescue). The proportions of these RGC classes were similar not only between control and *nob* rescue mice but also to our previously published data for C57Bl/6J mice (Sagdullaev and McCall 2005).

The RF center/surround organization of RGCs is generated by the interplay of excitatory and inhibitory inputs in both the inner and outer retina. As such, it is a sensitive measure of the normal synaptic organization of the retinal circuitry. To differentiate between the need for nyctalopin expression in the outer versus the inner retina, we quantitatively examined and compared the RF center size, surround antagonism, and the response gain for RGCs in control and *nob* rescue mice. Similar to controls, both ON- and OFF-center RGCs in *nob* rescue mice had well-defined RF centers and antagonistic surrounds. This result is evident in both the 3D response plots (Fig. 7, *A* and *B*) and in the ARFs from representative *nob* rescue and control RGCs (Fig. 7, *C* and *D*). The distributions of the RF center diameters, estimated from the optimal spot size of the ARF, of both ON- and OFF-center RGCs in *nob* rescue and controls overlap and their means are similar. In addition, the distributions of surround antagonism also were similar between control and *nob* rescue RGCs (Fig. 7,*E* and *F*; Table 1). Thus these hallmarks of the spatial extent of RGC RFs are indistinguishable between *nob* rescue and control mice and support the conclusion that nyctalopin expression in the OPL is sufficient to establish normal RGC function.

Our previous behavioral and ERG results showed that *nob* mice have a reduced ability to encode changes in light intensity (Gregg et al. 2003; Pardue et al. 1998). Therefore we quantitatively examined and compared response gain using IRFs in control and *nob* rescue RGCs as another measure of synaptic function in the retina (Chang et al. 2006; Sagdullaev et al. 2006). The average IRFs of both ON- and OFF-center *nob* rescue RGCs were the same as controls (Fig. 7, *G* and *H*) as were the quantitative measures of the dynamic range derived from these functions. Specifically, the maximum response, the intensity required to produce a half-maximum response and slope (Hill coefficients) of *nob* rescue RGCs did not differ from controls (Table 1).

These results show that the expression of the EYFP-nyctalopin fusion protein in the OPL, on the dendrites of the BCs, rescues all of the previously observed abnormalities in outer and inner retinal function of the *nob* mice, including the ERG b-wave and RGC spontaneous and evoked responses to full-field stimulation. The similarities in the quantitative characteristics of the spatial RF organization and response gain of RGCs in *nob* rescue and controls also strongly supports our hypothesis that nyctalopin expression is only critical at the level of DBC function in the retina and, that all other alterations in retinal function stem from this primary defect.

DISCUSSION

Our data show that expression of the EYFP-nyctalopin fusion protein only on DBC dendrites rescues visual function in both the outer and inner retina of *nob* mice. We interpret these results to indicate that nyctalopin plays a significant role in retinal processing only on the postsynaptic side of the photoreceptor to BC synapse. Thus these results settle several controversies in previously published results regarding the location of expression and the role of nyctalopin in retinal function.

Function of nyctalopin at the photoreceptor to BC synapse

The mutations in both *nob* mice and human patients with CSNB1 are likely to be null alleles. The mutation in *nob* mice is a deletion that causes a frame shift, which is predicted to destroy protein function (Gregg et al. 2003). In humans, >30 mutations have been identified (Bech-Hansen et al. 2000; Jacobi et al. 2002; Pusch et al. 2000; Zeitz et al. 2005a) and most are predicted to disrupt either the tertiary structure of the leucine rich repeat domains of nyctalopin or to truncate the protein (see review by Matsushima et al. 2005). A key question that remains is how mutations in the *Nyx* gene cause the observed defects in DBC signaling. Our patch-clamp data begin to shed light on this question. They show that even though in *nob* mice mGluR6 is localized appropriately on the BC dendrites (Ball et al. 2003; Fig. 3) glutamate application to the dendrites of DBCs is unable to mediate gating of the cation channel via the mGluR6 cascade (Fig. 1). In addition, these data provide new evidence that the nonspecific cation channel in *nob* DBCs is either closed or absent.

Nyctalopin is a member of the small leucine rich proteoglycans (Bech-Hansen et al. 2000; and Pusch et al. 2000; although see McEwan et al. 2006), and these proteins are involved in diverse functions including cell signaling, growth control, and formation of the extracellular matrix (see reviews by Hocking et al. 1998; McEwan 2006). In cultured cells, nyctalopin is expressed on the cell surface and attached by either a glycosyl phosphatidylinositol (GPI) anchor or a transmembrane domain, depending on species (O'Connor et al. 2005). Our EM data localize murine nyctalopin to the postsynaptic membrane and possibly the extracellular space and thus provides empirical support for these predictions. The questions of the exact role that nyctalopin plays in modulating the mGluR6 signal transduction cascade and how its loss disrupts signaling in this cascade remain unknown. The absence of nyctalopin expression does not lead to the loss or mislocalization of mGluR6 receptor expression (Ball et al. 2003; Fig. 3), thus it must have binding partners, either up or downstream of mGluR6 that provide a critical link(s) between these proteins, and the modulation of the nonspecific cation channel.

Rescue of outer and inner retina functional abnormalities in nob mice only requires expression of nyctalopin on BC dendrites

The ERGs of individuals with CSNB1 and *nob* mice clearly establish that an absence of nyctalopin causes abnormal transmission of the visual signal between photoreceptors and DBCs (Bech-Hansen et al. 2000; Krishna et al. 2002; Pardue et al. 1998; Pusch et al. 2000). Our results demonstrate that this defect is postsynaptic, and the absence of nyctalopin expression prevents glutamate induced responses in DBCs via mGluR6 modulation of a G-protein-coupled cascade that closes a nonspecific cation channel (see review by Duvoisin et al. 2005). In all other murine models of CSNB, the absence of a DBC response has been inferred from the absence of the ERG b-wave. Thus our results are the first direct verification of the absence of glutamate-induced signaling in DBCs and show definitively that the absence of an ERG b-wave is caused by the absence of signaling through the DBC and not the HBC pathway (Khan et al. 2005; Pardue et al. 1998) (Fig. 1).

The details of the DBC cascade that modulates the gating of the nonspecific cation channel remain poorly understood, although Gαo has been shown to play a role due to the absence of an ERG b-wave in knockout mice (Dhingra et al. 2000). Thus our findings clearly identify nyctalopin as a third critical element in the postsynaptic signaling cascade of the DBC pathway. Although nyctalopin's function remains unknown, it is not required for the expression and localization of either mGluR6 or Gαo because these proteins are expressed normally in *nob* retinas (Ball et al. 2003).

The restoration of RGC spontaneous and visually evoked response properties in *nob* rescue mice supports the hypothesis that normal retinal function only requires nyctalopin expression

on the DBC terminals postsynaptic to photoreceptors. All the response defects in *nob* RGCs, including abnormal spontaneous bursting and the disruption in visually evoked responses (Demas et al. 2006), are rescued by expression of EYFP-nyctalopin only in the dendrites of DBCs. Nyctalopin expression has been reported to be localized to many retinal layers and cell types, including robust expression in the IPL (Bahadori et al. 2006; Morgans et al. 2006; Pesch et al. 2003). Our data provide clear evidence at both the light and EM levels that the fusion protein is only expressed within or near the dendritic tips of DBCs in the OPL. Our results do not rule out expression of nyctalopin in other retinal cell classes because we used the $GABA_C$ ρ1 promoter to express EYFP-nyctalopin in BCs. Our electrophysiological results do, however, demonstrate expression beyond the OPL is not required for normal outer and inner retinal function. Thus we conclude that if nyctalopin is expressed outside of the OPL it is either redundant to another unknown protein or plays a very subtle role in RGC visual function that we failed to assess with our quantitative methods.

Localization of nyctalopin on BCs in the murine retina

Within the dendritic tips of BCs, EYFP-nyctalopin expression shows some co-localization with mGluR6, but also is located more proximal than mGluR6. Further, EYFP-nyctalopin is most frequently closely associated with the postsynaptic membrane. This location is consistent with the predictions and experimental evidence that nyctalopin is a small leucine rich proteoglycan (see review by Poopalasundaram et al. 2005). In *nob* rescue mice, EYFP-nyctalopin and mGluR6 are not associated with flat contacts on cone terminals, suggesting that nyctalopin is associated only with DBCs. This limited expression appears to occur despite the fact that $GABA_C$ receptors and GFP driven by the GABAc ρ1 promoter in another line of transgenic mice are expressed by both DBCs and HBCs. The absence of expression in HBCs could occur because of the lower expression of $GABA_C$ receptors in HBCs as compared with either rod or cone DBCs (Eggers et al. 2007). However, we believe a more likely explanation is that the absence of nyctalopin binding partners in HBCs results in a lack of targeting of the fusion protein and its subsequent degradation.

The *nob* mouse model recapitulates many of the features of human CSNB1. Because the underlying defect does not appear to involve anatomical abnormalities, it is possible that visual function in human patients might be improved using a gene therapy approach. However, in this study, the EYFP-nyctalopin protein in the transgenic mice was expressed early in retinal development (Demas et al. 2006). Therefore it will be important to determine if replacement of nyctalopin in adult *nob* mice can also restore function.

Acknowledgments

The authors thank C. Yee for the development of data collection and analysis software and S. Eichholtz for technical assistance.

GRANTS

This work was supported by National Eye Institute Grants EY-12354 to R. G. Gregg, EY-014701 to M. A. McCall, and EY014465 to N. S. Peachey, the Veterans Affairs Medical Research Service, and unrestricted grants from Research to Prevent Blindness.

REFERENCES

Artal P, Herreros de Tejada P, Munoz Tedo C, Green DG. Retinal image quality in the rodent eye. Vis Neurosci 1998;5:597–605. [PubMed: 9682864]

Bahadori R, Biehlmaier O, Zeitz C, Labhart T, Makhankov YV, Forster U, Gesemann M, Berger W, Neuhauss SC. Nyctalopin is essential for synaptic transmission in the cone dominated zebrafish retina. Eur J Neurosci 2006;24:1664–1674. [PubMed: 17004930]

Balkema GW Jr, Pinto LH. Electrophysiology of retinal ganglion cells in the mouse: a study of a normally pigmented mouse and a congenic hypopig-mentation mutant, pearl. J Neurophysiol 1982;48:968–980. [PubMed: 7143036]

Ball SL, Pardue MT, McCall MA, Gregg RG, Peachey NS. Immunohisto-chemical analysis of the outer plexiform layer in the nob mouse shows no abnormalities. Vis Neurosci 2003;20:267–272. [PubMed: 14570248]

Barthel LK, Raymond PA. Improved method for obtaining 3-microns cryo-sections for immunocytochemistry. J Histochem Cytochem 1990;38:1383–1388. [PubMed: 2201738]

Bech-Hansen NT, Naylor MJ, Maybaum TA, Sparkes RL, Koop B, Birch DG, Bergen AA, Prinsen CF, Polomeno RC, Gal A, Drack AV, Musarella MA, Jacobson SG, Young RS, Weleber RG. Mutations in NYX, encoding the leucine-rich proteoglycan nyctalopin, cause X-linked complete congenital stationary night blindness. Nat Genet 2000;26:319–323. [PubMed: 11062471]

Blanks JC, Johnson LV, Hageman GS. Stage-specific binding of peanut agglutinin to aggregates of degenerating photoreceptor cells in the rd mouse retina. Exp Eye Res 1993;57:265–273. [PubMed: 8224014]

Brinster RL, Chen HY, Trumbauer ME, Yagle MK, Palmiter RD. Factors affecting the efficiency of introducing foreign genes into mice by microin-jecting eggs. Proc Natl Acad Sci USA 1985;82:4438–4442. [PubMed: 3892534]

Chang B, Heckenlively JR, Bayley PR, Brecha NC, Davisson MT, Hawes NL, Hirano AA, Hurd RE, Ikeda A, Johnson BA, McCall MA, Morgans CW, Nusinowitz S, Peachey NS, Rice DS, Vessey KA, Gregg RG. The nob2 mouse, a null mutation in Cacna1f: anatomical and functional abnormalities in the outer retina and their consequences on ganglion cell visual responses. Vis Neurosci 2006;23:11–24. [PubMed: 16597347]

Demas J, Sagdullaev BT, Green E, Jaubert-Miazza L, McCall MA, Gregg RG, Wong RO, Guido W. Failure to maintain eye-specific segregation in nob, a mutant with abnormally patterned retinal activity. Neuron 2006;50:247–259. [PubMed: 16630836]

Dhingra A, Lyubarsky A, Jiang M, Pugh EN Jr, Birnbaumer L, Sterling P, Vardi N. The light response of ON bipolar neurons requires Gαo. J Neurosci 2000;20:9053–9058. [PubMed: 11124982]

Duvoisin RM, Morgans CW, Taylor WR. The mGluR6 receptors in the retina: analysis of a unique G-protein signaling pathway. Cell Sci Rev 2005;2:225–243.

Eggers ED, McCall MA, Lukasiewicz PD. Presynaptic inhibition differentially shapes transmission in distinct circuits in the mouse retina. J Physiol 2007;582:569–582. [PubMed: 17463042]

Enz R, Brandstatter JH, Wassle H, Bormann J. Immunocytochemical localization of the GABAc receptor ρ subunits in the mammalian retina. J Neurosci 1996;16:4479–4490. [PubMed: 8699258]

Ghosh KK, Bujan S, Haverkamp S, Feigenspan A, Wassle H. Types of bipolar cells in the mouse retina. J Comp Neurol 2004;469:70–82. [PubMed: 14689473]

Gregg RG, Mukhopadhyay S, Candille SI, Ball SL, Pardue MT, McCall MA, Peachey NS. Identification of the gene and the mutation responsible for the mouse nob phenotype. Invest Ophthalmol Vis Sci 2003;44:378–384. [PubMed: 12506099]

Hocking AM, Shinomura T, McQuillan DJ. Leucine-rich repeat glycoproteins of the extracellular matrix. Matrix Biol 1998;17:1–19. [PubMed: 9628249]

Jacobi FK, Andreasson S, Langrova H, Meindl A, Zrenner E, Pfelstedt-Sylla E, Pusch CM. Phenotypic expression of the complete type of X-linked congenital stationary night blindness in patients with different mutations in the NYX gene. Graefes Arch Clin Exp Ophthalmol 2002;240:822–828. [PubMed: 12397430]

Johnson LV, Hageman GS, Blanks JC. Interphotoreceptor matrix domains ensheath vertebrate cone photoreceptor cells. Invest Ophthalmol Vis Sci 1986;27:129–135. [PubMed: 3080382]

Khan NW, Kondo M, Hiriyanna KT, Jamison JA, Bush RA, Sieving PA. Primate retinal signaling pathways: suppressing ON-pathway activity in monkey with glutamate analogues mimics human CSNB1-NYX genetic night blindness. J Neurophysiol 2005;93:481–492. [PubMed: 15331616]

Kofuji P, Ceelen P, Zahs KR, Surbeck LW, Lester HA, Newman EA. Genetic inactivation of an inwardly rectifying potassium channel (Kir4.1 subunit) in mice: phenotypic impact in retina. J Neurosci 2000;20:5733–5740. [PubMed: 10908613]

Kozak M. An analysis of vertebrate mRNA sequences: Intimations of translational control. J Cell Biol 1991;115:887–903. [PubMed: 1955461]

Krishna VR, Alexander KR, Peachey NS. Temporal properties of the mouse cone electroretinogram. J Neurophysiol 2002;87:42–48. [PubMed: 11784728]

Lukasiewicz PD, Roeder RC. Evidence for glycine modulation of excitatory synaptic inputs to retinal ganglion cells. J Neurosci 1995;15:4592–4601. [PubMed: 7790926]

Masu M, Iwakabe H, Tagawa Y, Miyoshi T, Yamashita M, Fukuda Y, Sasaki H, Hiroi K, Nakamura Y, Shigemoto R. Specific deficit of the ON response in visual transmission by targeted disruption of the mGluR6 gene. Cell 1995;80:757–765. [PubMed: 7889569]

Matsushima N, Tachi N, Kuroki Y, Enkhbayar P, Osaki M, Kamiya M, Kretsinger RH. Structural analysis of leucine-rich-repeat variants in proteins associated with human diseases. Cell Mol Life Sci 2005;62:2771–2791. [PubMed: 16231091]

McCall MA, Lukasiewicz PD, Gregg RG, Peachey NS. Elimination of the ρ1 subunit abolishes GABA (C) receptor expression and alters visual processing in the mouse retina. J Neurosci 2002;22:4163–4174. [PubMed: 12019334]

McEwan PA, Scott PG, Bishop PN, Bella J. Structural correlations in the family of small leucine-rich repeat proteins and proteoglycans. J Struct Biol 2006;155:294–305. [PubMed: 16884925]

Miyake Y, Yagasaki K, Horiguchi M, Kawase Y, Kanda T. Congenital stationary night blindness with negative electroretinogram. A new classification. Arch Ophthalmol 1986;104:1013–1020. [PubMed: 3488053]

Morgans CW, Ren G, Akileswaran L. Localization of nyctalopin in the mammalian retina. Eur J Neurosci 2006;23:1163–1171. [PubMed: 16553780]

Nawy S, Jahr CE. Suppression by glutamate of cGMP-activated conductance in retinal bipolar cells. Nature 1990;346:269–271. [PubMed: 1695713]

O'Connor E, Eisenhaber B, Dalley J, Wang T, Missen C, Bulleid N, Bishop PN, Trump D. Species specific membrane anchoring of nyctalopin, a small leucine-rich repeat protein. Hum Mol Genet 2005;14:1877–1887. [PubMed: 15905181]

Ogden TE. The oscillatory waves of the primate electroretinogram. Vision Res 1973;13:1059–1074. [PubMed: 4197416]

Pardue, MT.; Ball, SL.; Candille, S.; McCall, MA.; Gregg, RG.; Peachey, NS. nob; a mouse model of CSNB1. In: Anderson, HR., editor. New Insights in Retinal Degenerative Disease. New York: Kluwer Academic/Plenum Publishers; 2001. p. 319-328.

Pardue MT, McCall MA, LaVail MM, Gregg RG, Peachey NS. A naturally occurring mouse model of X-linked congenital stationary night blindness. Invest Ophthalmol Vis Sci 1998;39:2443–2449. [PubMed: 9804152]

Pesch K, Zeitz C, Fries JE, Munscher S, Pusch CM, Kohler K, Berger W, Wissinger B. Isolation of the mouse nyctalopin gene nyx and expression studies in mouse and rat retina. Invest Ophthalmol Vis Sci 2003;44:2260–2266. [PubMed: 12714669]

Pinto LH, Vitaterna MH, Shimomura K, Siepka SM, Balannik V, Mc-Dearmon EL, Omura C, Lumayag S, Invergo BM, Glawe B, Cantrell DR, Inayat S, Olvera MA, Vessey KA, McCall MA, Maddox D, Morgans CW, Young B, Pletcher MT, Mullins RF, Troy JB, Takahashi JS. Generation, identification and functional characterization of a mutation in murine Grm6, nob4. Vis Neurosci 2007;24:111–123. [PubMed: 17430614]

Poopalasundaram S, Erskine L, Cheetham ME, Hardcastle AJ. Focus on molecules: nyctalopin. Exp Eye Res 2005;81:627–628. [PubMed: 16157331]

Pusch CM, Zeitz C, Brandau O, Pesch K, Achatz H, Feil S, Scharfe C, Maurer J, Jacobi FK, Pinckers A, Andreasson S, Hardcastle A, Wissinger B, Berger W, Meindl A. The complete form of X-linked congenital stationary night blindness is caused by mutations in a gene encoding a leucine-rich repeat protein. Nat Genet 2000;26:324–327. [PubMed: 11062472]

Robson JG, Frishman LJ. Photoreceptor and bipolar cell contributions to the cat electroretinogram: a kinetic model for the early part of the flash response. J Opt Soc Am A 1996;13:613–622.

Robson JG, Saszik SM, Ahmed J, Frishman LJ. Rod and cone contributions to the a-wave of the electroretinogram of the macaque. J Physiol 2003;547:509–530. [PubMed: 12562933]

Sagdullaev BT, McCall MA. Stimulus size and intensity alter fundamental response properties of mouse retinal ganglion cells in vivo. Vis Neurosci 2005;22:649–659. [PubMed: 16332276]

Sagdullaev BT, McCall MA, Lukasiewicz PD. Presynaptic inhibition modulates spillover, creating distinct dynamic response ranges of sensory output. Neuron 2006;50:923–935. [PubMed: 16772173]

Shiells RA, Falk G. Glutamate receptors of rod bipolar cells are linked to a cyclic GMP cascade via a G-protein. Proc Biol Sci 1990;242:91–94. [PubMed: 1706097]

van den Pol AN, Gorcs T. Synaptic relationships between neurons containing vasopressin, gastrin-releasing peptide, vasoactive intestinal polypeptide, and glutamate decarboxylase immunoreactivity in the suprachiasmatic nucleus: dual ultrastructural immunocytochemistry with gold-substituted silver per-oxidase. J Comp Neurol 1986;252:507–521. [PubMed: 2878014]

Vardi N, Duvoisin R, Wu G, Sterling P. Localization of mGluR6 to dendrites of ON bipolar cells in primate retina. J Comp Neurol 2000;423:402–412. [PubMed: 10870081]

Wachtmeister L, Dowling JE. The oscillatory potentials of the mudpuppy retina. Invest Ophthalmol Vis Sci 1978;17:1176–1188. [PubMed: 721390]

Wilson M, Tessier-Lavigne M, Attwell D. Noise analysis predicts at least four states for channels closed by glutamate. Biophys J 1987;52:955–960. [PubMed: 2447972]

Zeitz C, Minotti R, Feil S, Matyas G, Cremers FP, Hoyng CB, Berger W. Novel mutations in CACNA1F and NYX in Dutch families with X-linked congenital stationary night blindness. Mol Vis 2005a; 11:179–183. [PubMed: 15761389]

Zeitz C, van Genderen M, Neidhardt J, Luhmann UF, Hoeben F, Forster U, Wycisk K, Matyas G, Hoyng CB, Riemslag F, Meire F, Cremers FP, Berger W. Mutations in GRM6 cause autosomal recessive congenital stationary night blindness with a distinctive scotopic 15-Hz flicker electro-retinogram. Invest Ophthalmol Vis Sci 2005b;46:4328–4335. [PubMed: 16249515]

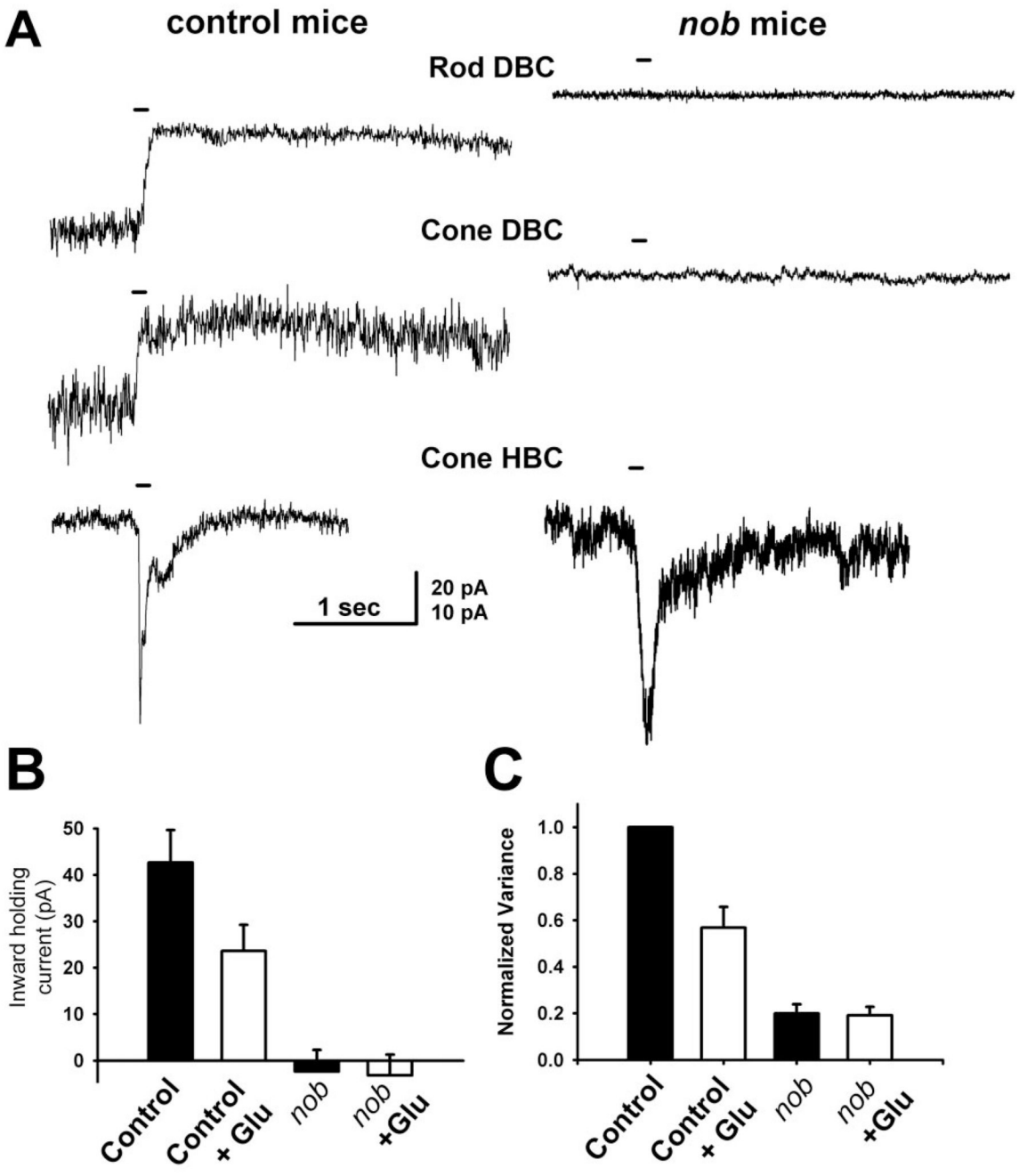

FIG. 1.

Depolarizing bipolar cells (DBCs) from *nob* mice do not respond to exogenous glutamate. *A*: responses of representative BCs to puffs of glutamate on their dendrites were recorded from control (*left*) and *nob* (*right*) mice, using whole cell voltage clamp (holding potential of −60 mV). In control slices, glutamate puffs elicited outward currents in rod ($n = 6$) and cone DBCs ($n = 4$) and inward currents in cone HBCs ($n = 2$). In *nob* retinal slices, responses to glutamate puffs never evoked a response in either rod ($n = 10$) or cone ($n = 9$) DBCs but evoked an inward current in all cone HBCs ($n = 5$), similar to controls. The bar over each current trace indicates the glutamate puff duration (100 ms). *B*: holding currents measured in either the absence or presence of glutamate in control and *nob* DBCs. Glutamate reduced the current in control mice

from −42.6 ± 6 to −23.6 ± 5.6 pA ($P < 0.003$) but did not affect the current in *nob* mice (2.4 ± 4.7 to 3.2 ± 4.5, $P = 0.52$). Currents in DBCs in both the absence ($P < 3 \times 10^{-5}$) and presence ($P < 0.0009$) of glutamate were significantly larger in control compared with *nob* mice. *C:* current variances, normalized to control in the absence of glutamate, were reduced by glutamate in control (from 1 to 0.57 ± 0.09, $P < 0.0008$), but not *nob* mice (from 0.20 ± 0.04 to 0.193 ± 0.04, $P = 0.47$). Current variances in both the absence ($P < 1 \times 10^{-11}$) or presence ($P < 0.002$) of glutamate were significantly larger in DBCs from control compared with *nob* mice. Calibration bar, 20 pA for rod and cone DBCs, 10 pA for cone HBCs, 1 s for all traces.

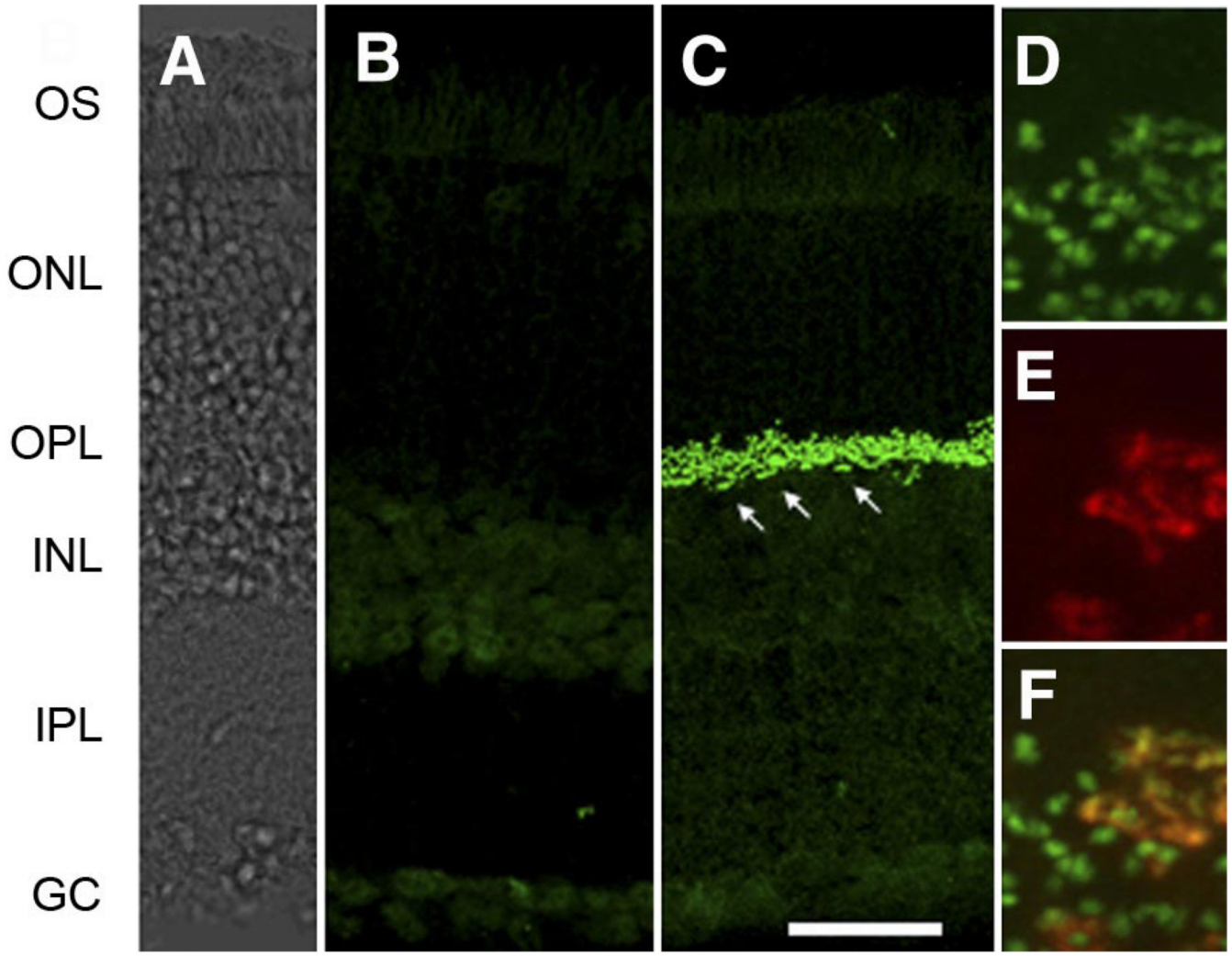

FIG. 2.

EYFP-nyctalopin fusion protein is expressed only in the outer plexiform layer (OPL) of *nob* rescue mice. *A*: DIC image of retina shown in *C. B* and *C*: representative transverse retinal sections from a control (*B*) and *nob* rescue mouse (*C*) stained for EYFP-nyctalopin, using anti-GFP antibodies. *D–F:* high-magnification images from transverse sections of *nob* rescue mouse showing staining of EYFP-nyctalopin (green, *D*), peanut agglutinin (PNA, red, *E*), and the merged image (*F*) These data show EYFP-nyctalopin is expressed at both cone (yellow) and rod (green) synapses. The arrows in *C* indicate cone terminals. Scale bar: *A–C* = 50 μm; *D–F* = 5 μm

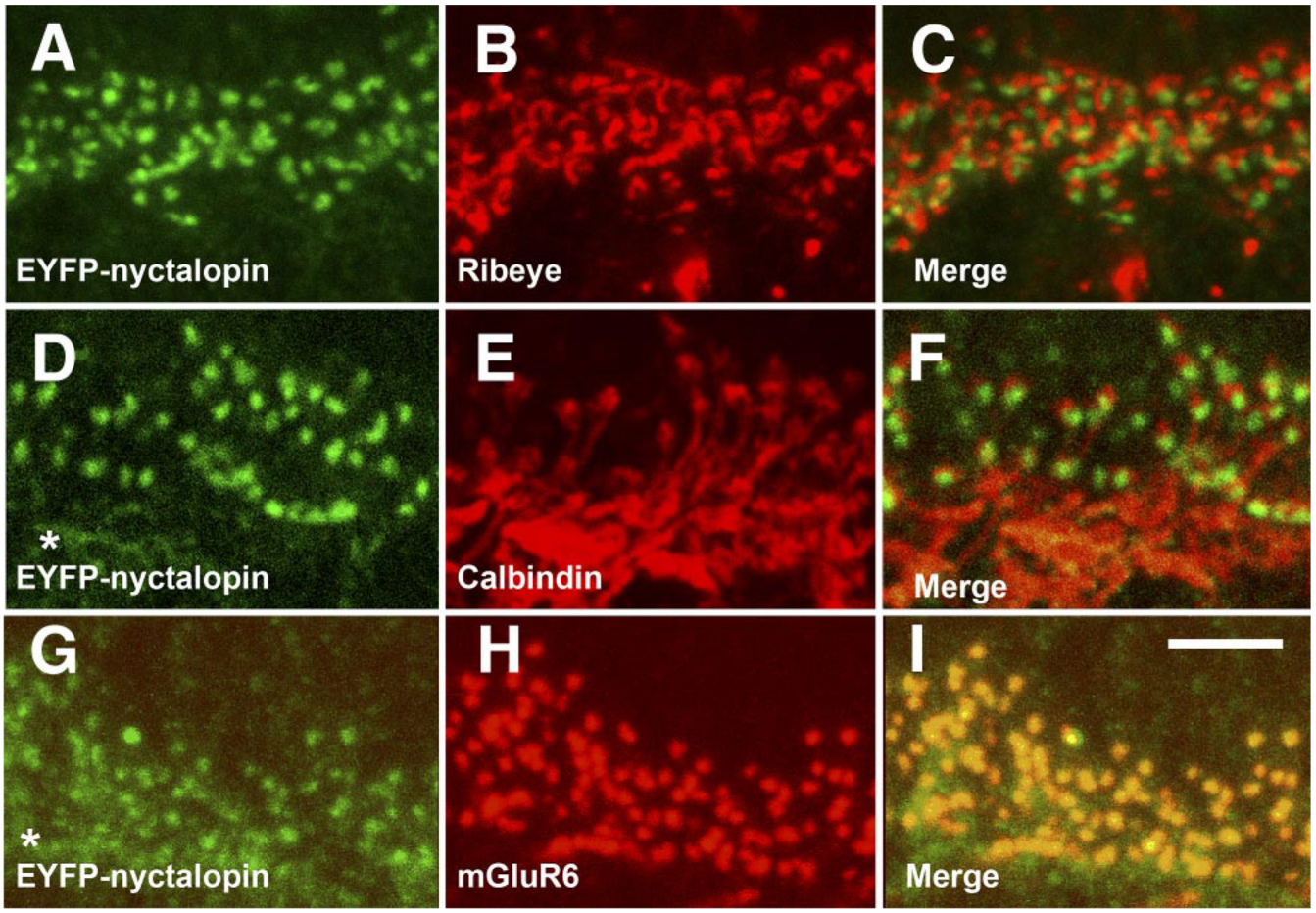

FIG. 3.

Expression of EYFP-nyctalopin in *nob* rescue retina is restricted to DBC dendritic terminals in the OPL. Staining of *nob* rescue retinal sections for EYFP-nyctalopin (green; *A*, *D*, and *G*) and ribeye (*B* and *C;* red), calbindin (*E* and *F;* red), and mGluR6 (*H*I; red). The merged images show that EYFP-nyctalopin is only co-localized with mGluR6 (*I*) but is closely aligned with both the presynaptic ribbon maker, ribeye (*C*) and the horizontal cell marker, calbindin (*F*). Scale bar = 5 μm.

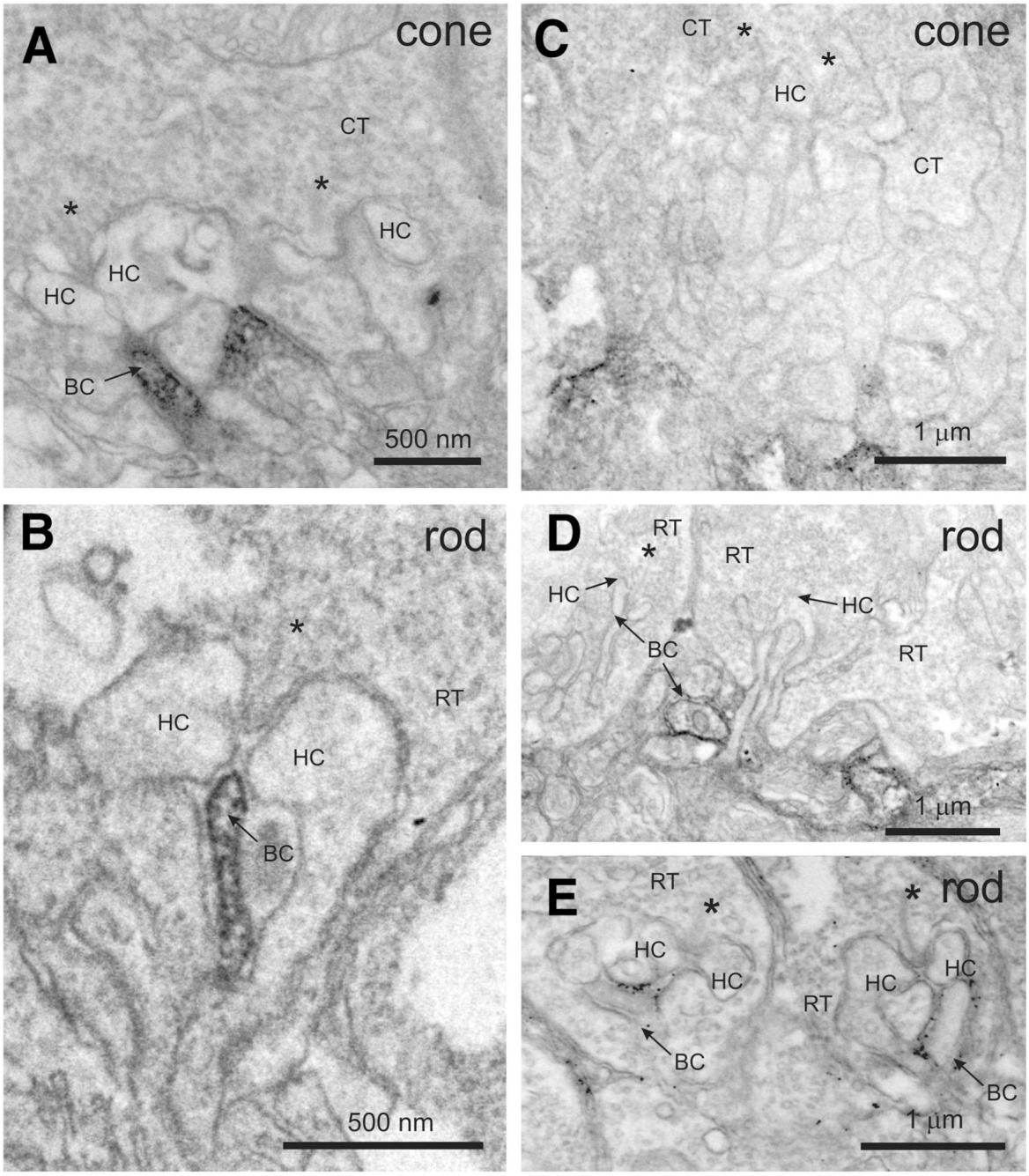

FIG. 4.

EYFP-nyctalopin is localized to the postsynaptic membrane of bipolar dendrites. Electron micrographs show staining for mGluR6 (*A* and *B*) and EYFP-nyctalopin (*C–E*) in *nob* rescue mice. Antibodies to mGluR6 stain invaginating processes of cone (*A*) and rod (*B*) photoreceptors. Antibodies to GFP stain EYFP-nyctalopin in *nob* rescue mice in or near cone (*C*) and rod (*D* and *E*) terminals. The staining of EYFP-nyctalopin is closely associated with cell membranes. Staining near cone terminals does not appear to involve the invaginating tip of the bipolar cells, rather it is slightly distal, at the base of the invagination. RT, rod terminal; CT, cone terminal, HC, horizontal cell dendrite; BC, bipolar cell dendrite; *, synaptic ribbon in rod and cone terminals.

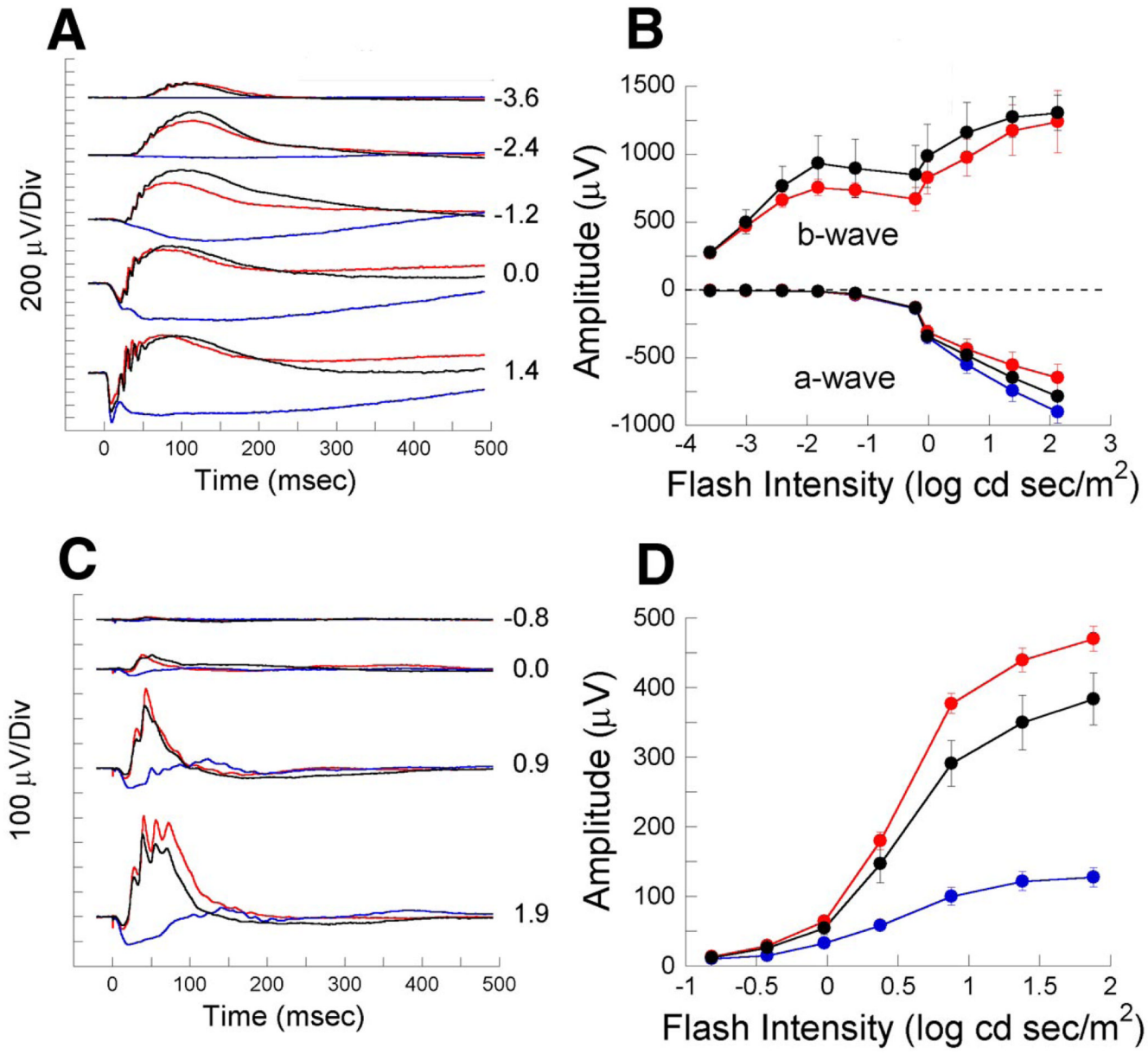

FIG. 5.

Expression of EYFP-nyctalopin on DBC dendrites restores the electroretinogram (ERG) b-wave in *nob* rescue mice. *A*: representative dark-adapted ERGs from control (black traces), *nob* (blue traces), and *nob* rescue (red traces) mice elicited by 5 flash intensities. Numbers indicate flash intensity in log cd s/m^2*B:* mean amplitudes ± SE of a- and b-waves from the ERGs of control, *nob*, and *nob* rescue mice (n = 4 mice in each group) at multiple flash intensities. *C*: representative light adapted ERG waveforms from the same mice as in *A* at 4 flash intensities. Numbers indicate flash intensity in log cd s/m^2*D*: mean amplitudes ± SE of ERG b-waves from these same mice.

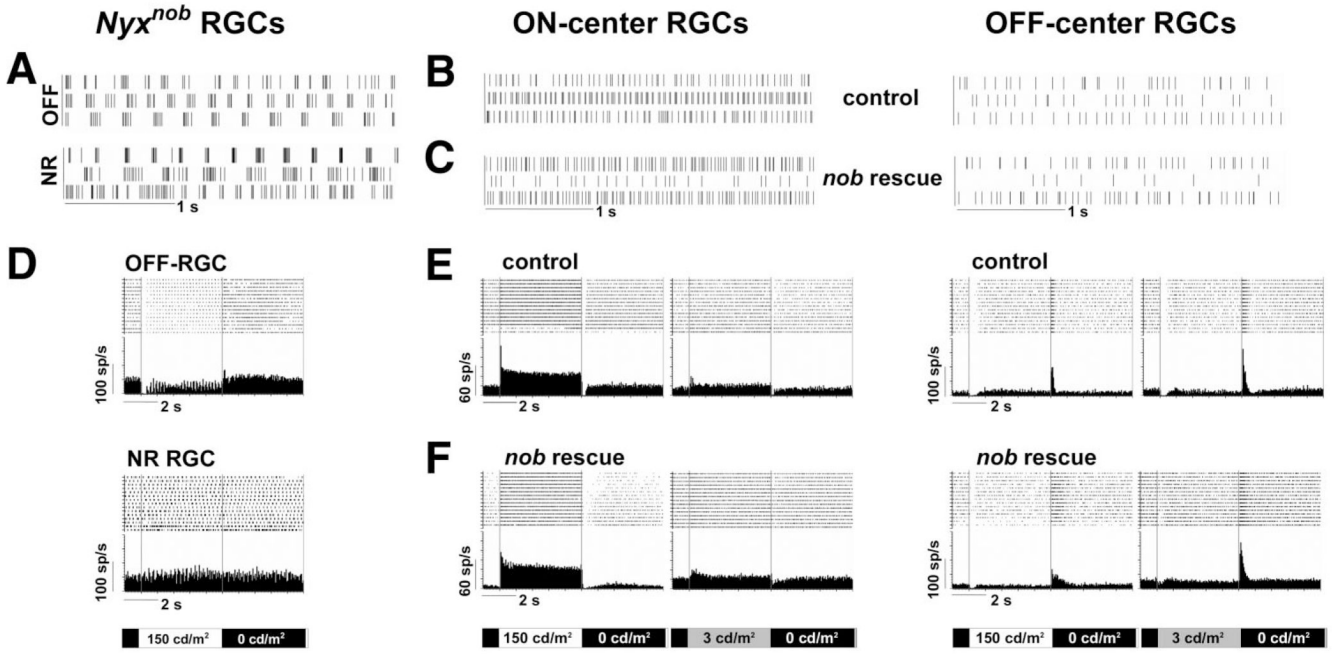

FIG. 6.

Spontaneous and light evoked responses of *nob* rescue retinal ganglion cells (RGCs) are identical to controls. *A–C*: raster plots of spontaneous activity in representative *nob*, control, and *nob* rescue RGCs under dark-adapted condition (0 cd/m^2). Each trace represents a different cell and shows that the bursting pattern is only present in *nob* RGCs. The lower spontaneous activity in OFF-center cells also is apparent in control and *nob* rescue mice. *D*: raster plots and PSTHs of 2 representative *nob* RGCs, 1 an OFF cell, and the 2nd that is not responsive to light stimuli. *E* and *F*: raster plots and average PSTHs of the evoked activity for representative ON- and OFF-center RGCs in control and *nob* rescue mice under both light (*left*; 0 to 150 cd/m^2) and dark (*right*; 0 to 3 cd/m^2) adapted conditions.

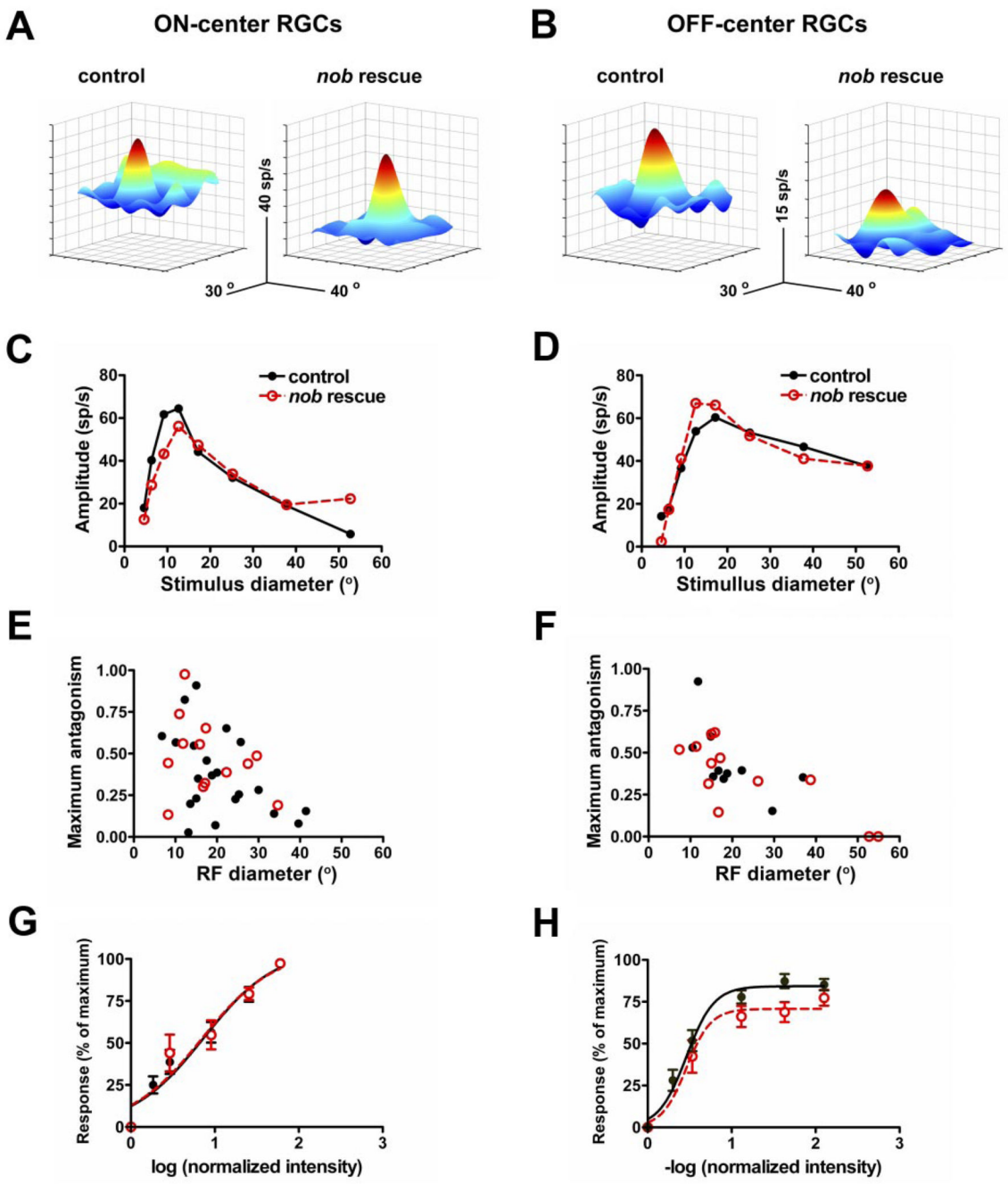

FIG. 7.

Center surround organization of RGCs from *nob* rescue mice are identical to controls. *A* and *B:* 3-dimensional depictions of receptive fields for representative ON- and OFF-center RGCs in control and *nob* rescue mice show robust receptive field centers (red) and antagonistic surrounds (blue). Responses in ON-center cells were elicited with bright spots (100 cd/m^2 presented on a 0 cd/m^2 background) and in OFF-center cells, dark spots (3 cd/m^2 on a 20 cd/m^2 background). *C* and *D:* area response curves for representative ON- and OFF-center RGCs in control (black) and *nob* rescue (red) mice show similar features that include: linear summation, a clear peak response and a falloff, that represents the contribution of the antagonistic response. From the area response curves, the receptive field diameter was estimated as the spot diameter

that produced the peak response and the receptive field surround contribution as the maximum antagonism index. *E* and *F:* plots of the optimal receptive field diameter as a function of maximum antagonism for each ON- and OFF-center RGCs recorded in control and *nob* rescue mice. The distributions of these parameters show complete overlap (see Table 1). Normalized intensity-response functions (IRFs) generated by center stimulation of ON (control, $n = 16$; *nob* rescue = 11)- and OFF (control, $n = 11$, *nob* rescue $n = 7$)-center RGCs in control (black) and *nob* rescue (red) mice are not different. For comparison, responses were normalized to the maximum response for each cell and plotted against the log (normalized intensity) where normalized intensity is the intensity of the light stimulus divided by the intensity of the adapting spot (30 cd/m^2). Sigmoidal curves were fit for each cell and used to estimate the maximum response, the intensity of light required to induce a half-maximal response (logEI50) and the slope (Hillslope) as a measure of dynamic range. No differences between control and *nob* rescue responses were observed in these measures (see Table 1).

TABLE 1

Response parameters of RGCs in control and nob rescue mice

	ON-Center		OFF-Center	
	Control	***nob* rescue**	**Control**	***nob* rescue**
ARF parameters	(21)	(13)	(10)	(12)
Center size,	20 ± 2	18 ± 2	19 ± 2.5	23 ± 5
Maximum antagonism	0.38 ± 0.05	0.48 ± 0.06	0.44 ± 0.07	0.36 ± 0.06
Maximum response, spike/s	58 ± 3	60 ± 5	86 ± 4	74 ± 11
IRF parameters	(16)	(11)	(11)	(7)
Normalized log intensity for	0.86 ± 0.14	0.85 ± 0.21	0.45 ± 0.03	0.48 ± 0.06
50% of maximum response	~212 cd/m^2	~217 cd/m^2	~11.3 cd/m^2	~12 cd/m^2
Hill coefficient	7.3 ± 0.2	7.1 ± 0.3	2.8 ± 0.6	3.0 ± 0.3

Student's *t*-tests of each of these response characteristics showed no significant differences between control and *nob* rescue parameters ($P > 0.05$ in all cases). Numbers of retinal ganglion cells (RGCs) in parentheses. Values are means ± SE.